Ecosystems (2020) 23: 1464–1480
https://doi.org/10.1007/s10021-020-00481-z

ECOSYSTEMS


# Characterizing Peatland Microtopography Using Gradient and Microform-Based Approaches

Jake D. Graham,[1]* Nancy F. Glenn,[1,2] Lucas P. Spaete,[3] and Paul J. Hanson[4]

[1]*Department of Geosciences, Boise State University, 1910 W University Dr, Boise, Idaho 83725, USA;* [2]*School of Civil and Environmental Engineering, The University of New South Wales, Sydney 2052, Australia;* [3]*Forestry Resource Assessment, Minnesota Department of Natural Resources, 483 Peterson Rd, Grand Rapids, Minnesota 55744, USA;* [4]*Climate Change Science Institute and Environmental Sciences Division, Oak Ridge National Laboratory, 1 Bethel Valley Rd, Oak Ridge, Tennessee 37830, USA*

## Abstract

Peatlands represent an important component of the global carbon cycle, storing 180–621 Gt of carbon (C). Small-scale spatial variations in elevation, frequently referred to as microtopography, influence ecological processes associated with the peatland C cycle, including *Sphagnum* photosynthesis and methane flux. Microtopography can be characterized with measures of topographic variability and by using conceptual classes (microforms) linked to function: most commonly hummocks and hollows. However, the criteria used to define these conceptual classes are often poorly described, if at all, and vary between studies. Such inconsistencies compel development of explicit quantitative methods to classify microforms. Furthermore, gradient-based characterizations that describe spatial variability without the use of microforms are lacking in the literature. Therefore, the objectives of this study were to (1) calculate peatland microtopographical elevation gradients and measures of spatial variability, (2) develop three microform classification methods intended for specific purposes, and (3) evaluate and contrast classification methods. Our results suggest that at spatial scales much larger than microforms, elevation distributions are unimodal and are well approximated with parametric probability density functions. Results from classifications were variable between methods and years and exhibited significant differences in mean hollow areal coverages of a raised ombrotrophic bog. Our results suggest that the conceptualization and classification of microforms can significantly influence microtopographic structural metrics. The three explicit methods for microform classification described here may be used and built upon for future applications.

**Key words:** peatland; microtopography; classification; terrestrial laser scanning; microform; microform classification; hummock; hollow; lidar.

## Highlights

- Digital elevation models of peatland microtopography were highly accurate
- Measures of surface roughness and elevation distributions were calculated
- Three microform classification schemes were developed and evaluated

Received 31 May 2019; accepted 9 January 2020;
published online 10 February 2020

**Electronic supplementary material:** The online version of this article (https://doi.org/10.1007/s10021-020-00481-z) contains supplementary material, which is available to authorized users.

**Corresponding author; e-mail:* jakegraham@u.boisestate.edu

## Introduction

Northern peatlands are an important component of the global carbon (C) cycle (Yu and others 2010, 2011), typically storing C at rates in the range of 20–30 g C $m^{-2}$ $y^{-1}$ (Yu and others 2011). Northern peatlands have been storing C for about 7000–14,000 years (Yu 2011; Morris and others 2018), resulting in total storage estimates ranging from 180 to 621 Gt C (Gorham 1990; Yu and others 2010; Yu 2012). The most recent estimate of 547 (473–621) Gt C from Yu and others (2010) represents over one-third of global terrestrial C, when using soil organic carbon estimates of about 1400 Gt C (Cao and Woodward 1998; Scharlemann and others 2014). Northern peatlands are also major contributors of atmospheric methane ($CH_4$) (Fung and others 1991). Methane emissions from Northern peatlands to the atmosphere (30–35 Tg $CH_4$ $y^{-1}$; Post and others 1982; Fung and others 1991; Gorham 1991) represent a significant source of atmospheric $CH_4$, with these emissions estimated to account for up to about 7% of global $CH_4$ emissions (Fung and others 1991).

The hummock–hollow complex dominates the microtopography of many peatlands and plays a major role in several ecological, hydrologic, and biogeochemical processes including C dynamics. Specifically, these include: an influence on greenhouse gas emissions (Bubier and others 2003; Hirano and others 2009; Moore and others 2011), rates of decomposition (Johnson and Damman 1991), peat accumulation (Chaudhary and others 2018), plant community (Andrus and others 1983; Chaudhary and others 2018; Harris and Baird 2018; Arsenault and others 2019; Malhotra and others 2016), plant productivity (Moore 1989), water chemistry (Arsenault and others 2019), and nutrient availability (Chapin and others 1979; Damman 1978). The primary biophysical driver of these differences is changes in peat water and oxygen content, which are associated with water table depth.

Water table depth is closely linked to multiple ecological processes associated with microtopography and biogeochemical cycling. The position of the water table controls where aerobic or anaerobic decomposition occurs in the peat column, which in turn influences carbon dioxide ($CO_2$) and $CH_4$ emissions (Moore and Dalva 1993). Anaerobic conditions beneath the water table drive $CH_4$ flux (Moore and Knowles 1989; Bubier and others 1993; Freeman and others 1993; Moore and Dalva 1993; Hirano and others 2009; Moore and others 2011; Munir and Strack 2014), and the water table has been described as an 'on–off switch' for $CH_4$ emissions by Christensen and others (2003). Furthermore, water content in non-vascular *Sphagnum* is linked to water table proximity (Rydin 1985), which modulates photosynthetic rates (Schipperges and Rydin 1998). Walker and others (2017) found water table depth to be a strong predictor of *Sphagnum* gross primary production (GPP) variability at the SPRUCE site (see below), due to the influence of water table depth on the vertical soil moisture gradient.

The predominantly saturated conditions in hollows promote anaerobic decomposition of organic material, which drives higher $CH_4$ emissions compared to hummocks (Moore and Knowles 1989; Bubier and others 1993). In contrast, hummocks exhibit higher $CO_2$ fluxes than hollows, because they occupy a larger fraction of the peat column in aerobic conditions and can experience warmer temperatures seasonally, influencing rates of $CO_2$ emission (Moore and Knowles 1989; Bubier and others 1993). Although the ratio of emitted $CO_2$:$CH_4$ differs between microforms, $CO_2$ flux is higher than $CH_4$ flux in both microforms (Kim and Verma 1992; Bubier and others 1993; Waddington and Roulet 1996).

Methods that provide robust datasets for characterizing peatland microtopography and classifying microforms were lacking until recently, resulting in descriptions ranging from qualitative (for example, Bubier and others 1993; Nungesser 2003; Benscoter and others 2005) to quasi-quantitative (for example, Johnson and others 1990; Weltzin and others 2001; Pouliot and others 2011). Examples of qualitative descriptors for hollows include elevation (low areas), slope (flat areas), and concavity (depressions). Ambiguous descriptions can confound classifications of microforms between studies. Moreover, explicit quantitative definitions provide clarity and allow for improved scaling and syntheses between studies.

One reason for the lack of detailed quantitative characterizations of peatland microtopography was the previous inability to provide dense and highly accurate elevation data to measure microtopography over large areas (for example, Almendinger and others 1986; Huang and others 1988; Huang and Bradford 1990; Ehrenfeld 1995; Flanagan and others 1995; Darboux and Huang 2003; Pouliot and others 2011). Recently, however, remote sensing technologies including unmanned aerial systems (UAS) based structure from motion (SfM) (Lucieer and others 2014; Mercer and Westbrook 2016; Smith and others 2016; Nouwakpo and others 2014; Smith and Warburton 2018; Moore and

others 2019) and terrestrial laser scanning (TLS) (Barneveld and others 2013; Brubaker and others 2013; Nouwakpo and others 2016) have been used to measure microtopography. Terrestrial laser scanning is a remote sensing technology that provides accurate and dense point clouds, providing a promising technique for characterizing peatland microtopography at fine scales over relatively large areas (for example, 0.01–0.10 m resolution over 10–100 s of meters). Stovall and others (2019) used TLS to generate high-resolution digital elevation models (DEM) of wetland microtopography with high accuracy (root-mean-squared error; RMSE = 0.04 cm) and used a topographic segmentation algorithm to define hummock microforms. Additionally, Moore and others (2019) used SfM to derive digital models of peatland microtopography and used Gaussian mixed models to characterize elevation distributions of microtopography.

Considering the influence of microtopography on hydrologic and biogeochemical processes, proper representation of microtopography in land surface models is needed for accurate simulations of biogeochemical cycles (see Moore and others 2019). Most land surface models do not accurately characterize C emissions from peatlands, partially because they do not represent peatland microtopography or hydrology. However, several models have been made, or modified, to incorporate peatland microtopography (Frolking and others 2002; Baird and others 2011; Morris and others 2011a, b; Shi and others 2015). Some models utilize simplistic approaches that represent discrete hummock and hollow microforms (Frolking and others 2002; Shi and others 2015), whereas DigiBog (Baird and others 2011) provides a more sophisticated approach that is able to incorporate elevation gradients representative of peatland microtopography.

The incorporation of microtopography in both field and modeling studies that investigate the hydrology, ecology, and biogeochemistry of peatlands compels the need for accurate characterization of microtopography. Characterization of microtopography should include methods that retain high structural fidelity and resolution, in addition to quantitative microform classifications intended for implementation into applications using the hummock–hollow dichotomy. Therefore, the objectives of this study were to (1) calculate and analyze measures of microtopography with high structural fidelity (that is, elevation distributions, surface roughness, and spatial variation), (2) develop and assess three application-specific microform classification methodologies, and (3) compare classification results using the three methods and discuss their utility for both modeling and field studies. To accomplish these objectives, we utilized TLS measured point clouds to derive high-resolution DEMs of the bog. We then calculated measures of surface roughness and model semivariograms and finally performed quantitative microform classifications on the generated DEM to produce spatially explicit maps of microforms for comparison.

## Methods

### Study Site

The Spruce and Peatland Response Under Changing Environments project (SPRUCE; Hanson and others 2017b) experiment is located at the S1 bog in the Marcell Experimental Forest, Northern Minnesota, USA. The S1 bog is an 8.1 ha ombrotrophic peat bog with a perched water table and little regional groundwater influence (Sebestyen and others 2011). Mean annual air temperature at S1 was 3.4°C, and mean annual precipitation was 780 mm between 1969 and 2009 (Sebestyen and others 2011). S1 is acidic (near surface pore water pH $\approx$ 3–4) with an average peat depth of 2.27 m and basal age of the deepest centimeter of peat profiles ranging from 5100 to 11,100 cal BP (Slater and others 2012; Griffiths and Sebestyen 2016; McFarlane and others 2018). Additional details about the study site can be found in Sebestyen and others (2011).

The undulating hummock–hollow surface of the S1 bog was the basis for the analyses in this paper. Access to experimental plots (nominally 12 m diameter) throughout the S1 bog was provided by a network of boardwalks installed for the SPRUCE experiment (Hanson and others 2017b). Twelve plots were selected for scanning using TLS. Ten of the SPRUCE plots were enclosed for warming treatments, and two were open ambient plots. Each plot was surrounded by an octagonal boardwalk that formed the stable base from which TLS scans were obtained.

### TLS Scans

All scans were collected using a Riegl VZ-1000 terrestrial laser scanner, which utilizes a 1550 nm laser to produce a three-dimensional representation of the surrounding area (point cloud; Figure 1A). Four TLS scans were taken per SPRUCE plot and subsequently registered together in RiSCAN PRO to produce a single point cloud for each SPRUCE plot (Graham and others 2019a). The

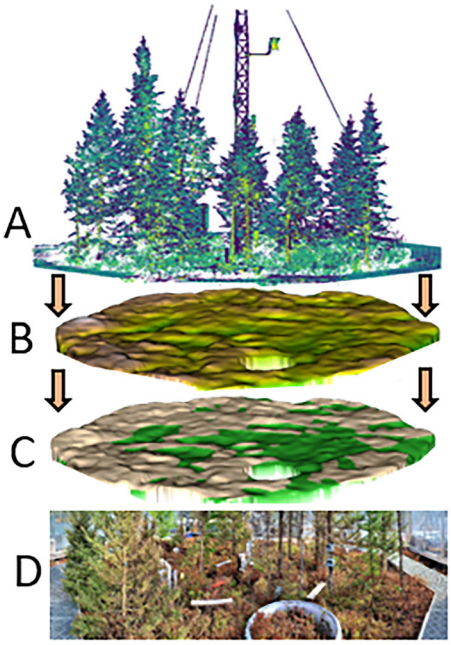


**Figure 1.** Workflow used to generate microform classification maps, starting with the terrestrial laser scanning point cloud (A; colored by intensity) used to generate the digital surface model (B; colored by elevation), and finally the microform classification map (C; colored by microform). SPRUCE plot 10 is used as an example. Additionally, an image of the mapped domain (D) showing one of the large flux collars that occluded laser scanner pulses and caused the ''holes'' in maps. Spatial scales between panes (A, B, C) are not exact; however, horizontal and vertical scales are 1:1 in individual panes.

SPRUCE plots were scanned in April–May of 2016, 2017, and 2018, with an angular resolution of 0.04 degrees. Scanning was performed early in the year following snowmelt so that the bog surface was not obscured by later development of shrub-layer canopies of plant foliage.

## Surface Reconstruction

Point clouds were processed to retain points within the boardwalk (~ 9 m edge-to-edge) of each SPRUCE plot. Small areas within the scanned plot were occupied by large flux collars (Hanson and others 2017a) that inhibited laser pulses from assessing the bog surface and were excluded from the analysis. To reconstruct the bog surface, the data were filtered to extract the lowest return in a 2D grid, with grid cells measuring 0.1 × 0.1 m. A surface mesh was created using the Poisson surface reconstruction (Figure 1B) (Kazhdan and others 2006) plugin for CloudCompare v2.8 (CloudCompare 2017), which is capable of reconstructing surfaces from noisy data. This mesh was sampled to discretize the surface and generate a DEM with 0.01 m grid cells (Graham and others 2019b). DEMs in this study primarily represent the top of *Sphagnum* capitula. In locations where there was no *Sphagnum* coverage, DEMs represent the top of other low stature vegetation (for example, feather mosses) or bare earth.

## Surface Roughness and Elevation Variability

Quantitative characterizations of peatland microtopography in the literature are sparse, although model representations that can utilize detailed topographic data including elevation distributions, such as DigiBog, are currently in use (Baird and others 2011). Further, elevation distributions can be used in conjunction with measures of biogeochemical processes made along an elevation, or the associated water table depth, gradient (for example, Moore and Knowles 1989; Bubier and others 1993, 2003; Moore and others 2011) to make spatial extrapolations of quantities of interest. Therefore, providing characterizations of microtopography that are related to elevation gradients and spatial variability will help improve model simulations of peatland dynamics and facilitate more accurate estimates of biogeochemical fluxes. In this study, we provide four measures of microtopography in SPRUCE plots (for the 2017 dataset) that are based on elevation distributions, spatial variability, and surface roughness of peatland microtopography.

### *Elevation Distributions*

Elevation distributions were unimodal and fairly well approximated by normal distributions; however, elevation distributions were typically skewed left and had positive kurtosis (Figure 2). Therefore, we utilized Pearson's distributions (Pearson 1895, 1901, 1916; Johnson 1949) to represent elevation distributions to deal with skewness and kurtosis. The Pearson distributions are a family of probability distributions which use 2–4 parameters to generate continuous probability density functions. The type of Pearson's distributions and the parameters were calculated using the ''pearsonFitML'' function in the Program R (R Core Team 2017) package ''PearsonDS''. Distributions were fit to the twelve SPRUCE plots individually and combined.

### *Random Roughness*

Random roughness (RR) and its variants are among the simplest and most commonly used surface

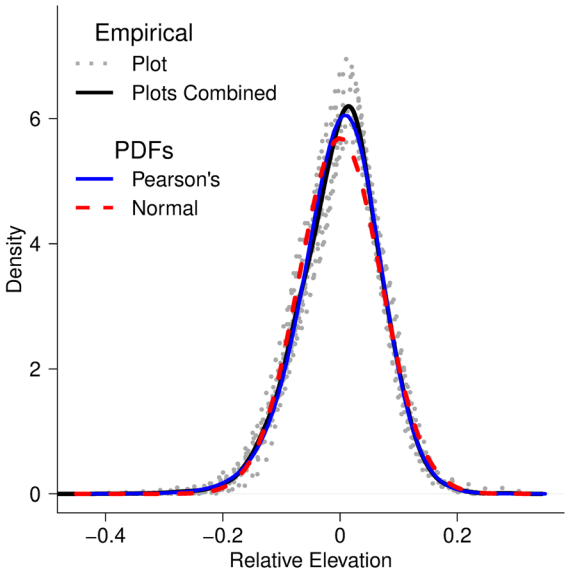


**Figure 2.** Elevation distributions for individual SPRUCE plots; also displaying the distribution for all SPRUCE plots combined with fit normal and Pearson's distributions.

roughness metric which refer to measures of variation in elevation without consideration for the spatial arrangement of roughness elements. Previous studies have used both standard error (Allmaras and others 1966; Currence and Lovely 1970) and standard deviation ($\sigma$) (Kamphorst and others 2000; Moreno and others 2008; Vermang and others 2013) as measures of variability. Here, we calculate RR as $\sigma$ of elevation from the DEM cells for the twelve individual SPRUCE plots and plots combined.

### *DEM Roughness Length*

Roughness length ($z_0$) is a measure of surface roughness, which is used to characterize microtopography (Campbell and others 2002; Brubaker and others 2013) that is a representation of roughness elements and corresponds to the point at which the wind speed is zero in the log wind profile. Therefore, $z_0$ can be used to represent the influence of microtopography on turbulence and the resulting effect on surface mass and energy fluxes (Choudhury and others 1979; Campbell and others 2002). Studies using $z_0$ have calculated the parameter in many ways, from calculating using RR and simple transect-based approaches (Kuipers 1957; Lettau 1969), to more sophisticated DEM and point cloud approaches (Smith and others 2016; Miles and others 2017). Here, we calculate $z_0$ using the DEM method described in Smith and others (2016) for each of the twelve SPRUCE plots.

### *Model Semivariograms*

Semivariograms describe the spatial correlation of random data fields, and when applied to elevation can be used to describe topographic morphology and surface roughness (Darboux and others 2002; Smith and Warburton 2018). Empirical semivariograms plot the semivariance against the lag distance separating points (Figure 3), and the model semivariogram can be fit to the empirical semivariogram using three parameters: range ($r$), sill ($s$), and nugget ($n$). In this study, we fit exponential model variograms to empirical semivariograms consisting of 10,000 random samples from each SPRUCE plot. Our sampling intervals were sufficiently small, and $n$ appeared to be absent or extremely small in empirical semivariograms; therefore, we set $n$ in all model variograms to zero. Parameters $s$ and $r$ were calculated for each SPRUCE plot and combined.

## Microform Classification Methods

Hollows can qualitatively be defined as low areas, or depressions within the peatland that are often in close proximity to the water table relative to the surrounding area. Hummocks are defined as higher mounds rising above the hollows, which results in perched peat/root complexes that are further from the water table. For applications that utilize stratified sampling of each microform (for example, Kim and Verma 1992; Waddington and Roulet 1996; Sullivan and others 2008), such definitions may be

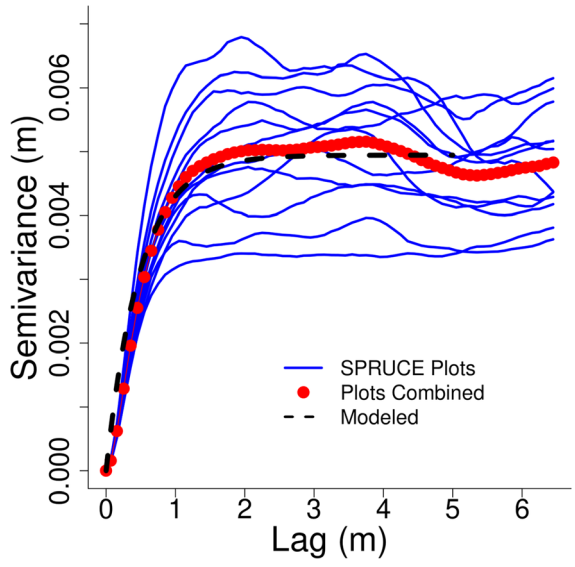


**Figure 3.** Empirical semivariograms for individual SPRUCE plots, also displaying the empirical and associated model semivariogram for all plots combined.

sufficient, because investigators can select areas to sample that most embody these qualitative definitions. However, subjective selection of sampling points in the most representative areas (that is, extremes of both microforms, top of hummocks, and bottom of hollows) is inadequate to quantitatively scale small-footprint measured data across the complete landform (see Moore and others 2019). Further, these qualitative descriptions lack sufficient detail to classify microforms from a DEM.

Modeling studies utilizing simplified two-column approaches to microtopography, for example Shi and others (2015) and Frolking and others (2002), represent microforms as soil columns which are differentiated by elevation. In contrast, field investigators placing instrumentation may consider qualitative metrics in addition to elevation (for example, mounds, depression-like, transitional slopes, and flat or planar areas). This demonstrates that the conceptualization of microforms is application specific, and therefore, so should classification schemes.

Microform classification schemes should target specific objectives and be explicitly defined, as to not confound analyses spanning multiple studies. Stovall and others (2019) marks a major advance toward more useful methods to quantify wetland microforms; however, the study used subjective manual delineations of hummocks as validation data. To address the need for explicit microform classification schemes, we developed quantitative methods to classify microforms for three purposes that differ in their conceptualize of microforms (a) the Functional_Classification classifies microforms based on how the structure of microtopography interacts with ecological drivers to determine ecological function; (b) the ELM_Classification is designed to generate microtopographic parameters that are most consistent with the conceptualization of microtopography in a land surface model, ELM_SPRUCE (see below); and (c) the Scaling_Classification is constructed to classify microforms in a manner consistent with the subjective placement of instrumentation in the field, and meant to be used to make spatial extrapolations. To accommodate each of these applications, classification methodologies were customized to be best suited for each individual application. For Functional_Classification, we incorporated water table depth data so that classifications using this method would be representative of ecological function, rather than simply reflect structure. To provide the best estimates of microtopographic model parameters, ELM_Classification only considers relative elevation, which is consistent with the representation of microtopography in the model. Scaling_Classification is intended to be used for scaling point, or small footprint, measurements to larger spatial extents. Therefore, it attempts to classify peatland microtopography in a manner most consistent with the placement of instrumentation by researchers in the field.

## Method 1: Functional_Classification

We used depth to water table as a link to ecological function and as a classification metric, because it is related to multiple ecological processes including *Sphagnum* photosynthesis and $CH_4$ flux. Water table is measured at each SPRUCE plot. Thus, we used the plot-specific daily mean warm-season median water table (WSMWT hereafter) and a tolerance for a classification threshold for microforms (Figure 4). The warm, or ice-free, season was defined as the period when air temperatures remained above 0°C. This classification method differs from the two others, because microform coverage can change annually even if there is no change to the structure of the microtopography. This enables us to classify microforms to represent changes in ecosystem function incurred by changes in water table depth. For instance, increased evapotranspiration in the warmest SPRUCE plots (+9°C) may cause areas that would typically function in a hollow-like manner to function more like hummocks because of lower water tables due to drying.

Microform class was determined by whether the elevation was above or below the WSMWT plus the tolerance, as shown in Eq. 1:

$$C_{\mathrm{F}}(x,y) = \begin{cases} \mathrm{Hu}, & \text{if } z_{xy} \geq (zwt_{p50} + \mathrm{Tol}) \\ \mathrm{Ho}, & \text{if } z_{xy} < (zwt_{p50} + \mathrm{Tol}) \end{cases} \quad (1)$$

where $x$ and $y$ are geospatial coordinates (that is, northing and easting), $C_F(x,y)$ is the Functional_Classification at location $xy$, Hu and Ho are hummock and hollow classifications, respectively, $z_{xy}$ is the elevation at location $xy$, $zwt_{p50}$ is the plot-specific WSMWT, and Tol is a tolerance in meters.

The tolerance for elevations above WSMWT (0.10 m) was chosen based on desiccation levels of hollow-associated *Sphagnum* species relative to water table, and productivity relative to water content reported in Rydin (1985) and Schipperges and Rydin (1998), respectively. Rydin (1985) reports species of *Sphagnum* associated with hollows reach a water content of ≈ 750% (percent of dry weight) at a distance of ≈ 0.10 m from the water table, and this level of water content is associated with a sharp drop in *Sphagnum* photosynthesis

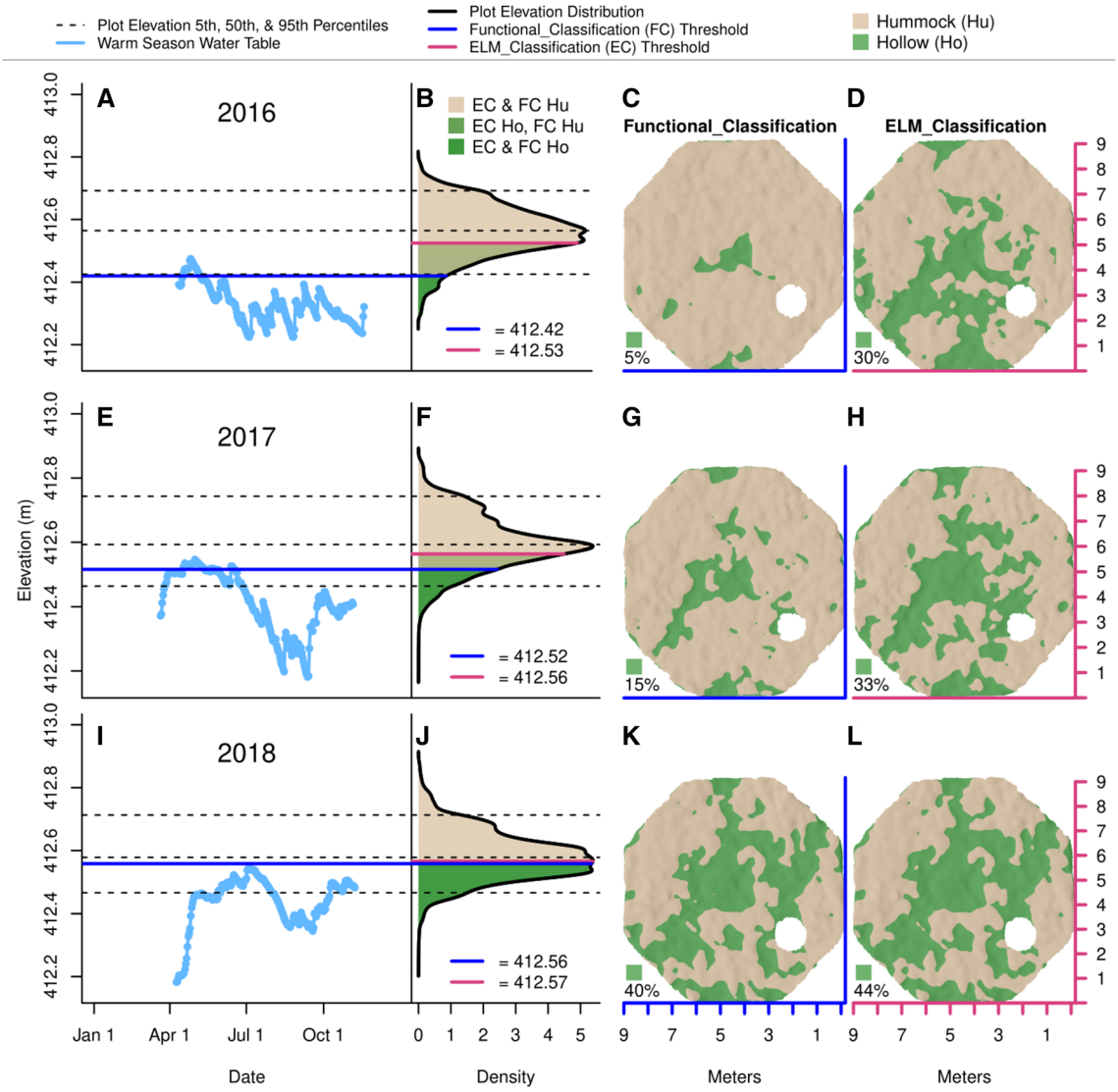


**Figure 4.** Warm-season water table (**A**), plot of digital surface model elevation distribution (**B**), and maps of classified microforms resulting from the thresholds displayed in B for the Functional_Classification and ELM_Classification (**C**, **D**, respectively) for SPRUCE plot 8 in 2016. The same is displayed for 2017 (**E**–**H**) and 2018 (**I**–**L**). To facilitate comparisons, plot elevation distributions (**B**, **F**, **J**) are displayed with elevation on the *y*-axes consistent with axes on warm-season water tables plots (**A**, **E**, **I**).

(Schipperges and Rydin 1998). This (0.1 m) is also the depth at which Christensen and others (2003) suggested $CH_4$ emission is ''turned on'' or off, based on data from Greenland, Iceland, Scandinavia, and Siberia. While this ''on–off switch'' for $CH_4$ emissions may not be representative of all peatlands, the 0.10 m from Christensen and others (2003) is derived from five sites on multiple continents, and thus is likely representative of northern peatlands over a broad geographic region. Therefore, a 0.10 m tolerance above the WSMWT represents an elevation threshold at which areas below should function ecologically like a hollow for at least half of the warm-season and is used to classify microforms.

## Method 2: ELM_Classification

Shi and others (2015) have recently created a modified version of the Energy Exascale Earth System Model (E3SM) land model (ELM) that represent the hydrology and microtopography of peatlands. This modified version of ELM (referred to as ELM_SPRUCE) was created based on experiments at the SPRUCE site. ELM_SPRUCE uses a two-column approach to peatland microtopography, where one column is representative of hum-

mocks and the other of hollows (similar to the representation in Frolking and others 2002). These columns have identical soil and PFT properties and only vary in elevation and water table depth. Modifications made by Shi and others (2015) included the representation of near surface flow from hummock to hollow, lateral drainage to the lagg, and the glacial till acting as a barrier to vertical and lateral drainage. Shi and others (2015) reported improved simulations of water table position but did not simulate biogeochemistry in ELM_SPRUCE. However, they state that peatland hydrology influences peatland C dynamics, and therefore these modifications to the hydrologic cycle will affect C cycling.

The ELM_SPRUCE approach to microtopography uses three uncertain parameters in the representation of microtopography: hummock–hollow height differential (0.3 m), hummock–hollow horizontal separation (1.0 m), and proportional cover of each microform (25% hollow; Shi and others 2015). The current default values for these parameters were obtained heuristically, and therefore the accuracy and uncertainty of the values are largely unknown. In this paper, we developed methods that facilitate quantitative evaluation of such representations of microtopography, and their parameters.

A method using only information from the plot elevation distribution was used for a classification scheme to represent microtopography in a manner most consistent with how microtopography is represented in ELM_SPRUCE. Hummocks and hollows are represented in the model as soil columns that, other than elevation, have identical properties. Therefore, it is most consistent to classify microforms based on structure alone (elevation), and not include the water table position, because it is simulated explicitly in ELM_SPRUCE. While similar techniques could be used for other models, we chose to focus on ELM_SPRUCE, because it is configured based on the SPRUCE site and because it is able to couple to the Earth system model E3SM.

An elevation threshold was used for classification as a vertical tolerance from the plot elevation fifth percentile, where any points below the elevation threshold were classified as hollow and points above were classified as hummock (Figure 4). Explicitly:

$$C_{\mathrm{ELM}}(x,y) = \begin{cases} \mathrm{Hu}, & \text{if } z_{xy} \geq (z_{p5} + \mathrm{Tol}) \\ \mathrm{Ho}, & \text{if } z_{xy} < (z_{p5} + \mathrm{Tol}) \end{cases} \quad (2)$$

where $C_{\mathrm{ELM}}(x,y)$ is the ELM_Classification at location $xy$, $z_{p5}$ is the plot-specific elevation fifth percentile, and Tol is a tolerance in meters. The fifth percentile is intended to represent the elevation at the bottom of a 'typical' hollow and was used instead of the plot minimum to mitigate any effect of extremely or erroneously low points. The tolerance used for the final classification was 0.10 m.

## Method 3: Scaling_Classification

We created an index to classify microforms (Hollow Index) based on elevation, concavity, and slope. Considering researchers in the field often do not have access to metrics like the MWSWT or the elevation fifth percentile, these metrics are meant to be the quantitative counterparts to qualitative descriptors used by field researchers to identify microforms. This method, therefore, is aimed to provide classifications consistent with researchers identifying microforms in the field and best suited for scaling stratified measurements. For example, if we took stratified measurements of $CH_4$ flux in both hummocks and hollows, and wanted to make a bog-scale estimate of $CH_4$ flux, we would need to know the areal coverage of each microform. The Scaling_Classification method is aimed to provide microform areal coverages best suited for spatial extrapolations of similar stratified field measurements.

The Hollow Index is a product of the three metrics, after being passed through sigmoidal weighting functions (Figure 5). Sigmoid weighting functions are parameterized to accentuate ''hollow-like'' characteristics (that is, low elevation, positive concavity, and relatively flat). The output of the Hollow Index is a continuous variable (Figure 6A, B), in which higher positive values correspond to the most hollow-like areas. Therefore, a threshold was applied to the Hollow Index to produce microform classification maps (Graham and others 2019b). Thresholding for classifications can be application/user specific. Based on iterative thresholding, we used 2.2 as our threshold (Figure 6C, D). Additional information and methods related to the parameterization of sigmoid weighting functions in the Hollow Index and Scaling_Classification can be found in the Supplemental Material.

## Statistics

To evaluate the variability in hollow percent cover for a given plot across the 3 years (for example, inter-annual (intra-plot) variability), we calculated the $\sigma$ of percent cover for hollows for the 3 years of

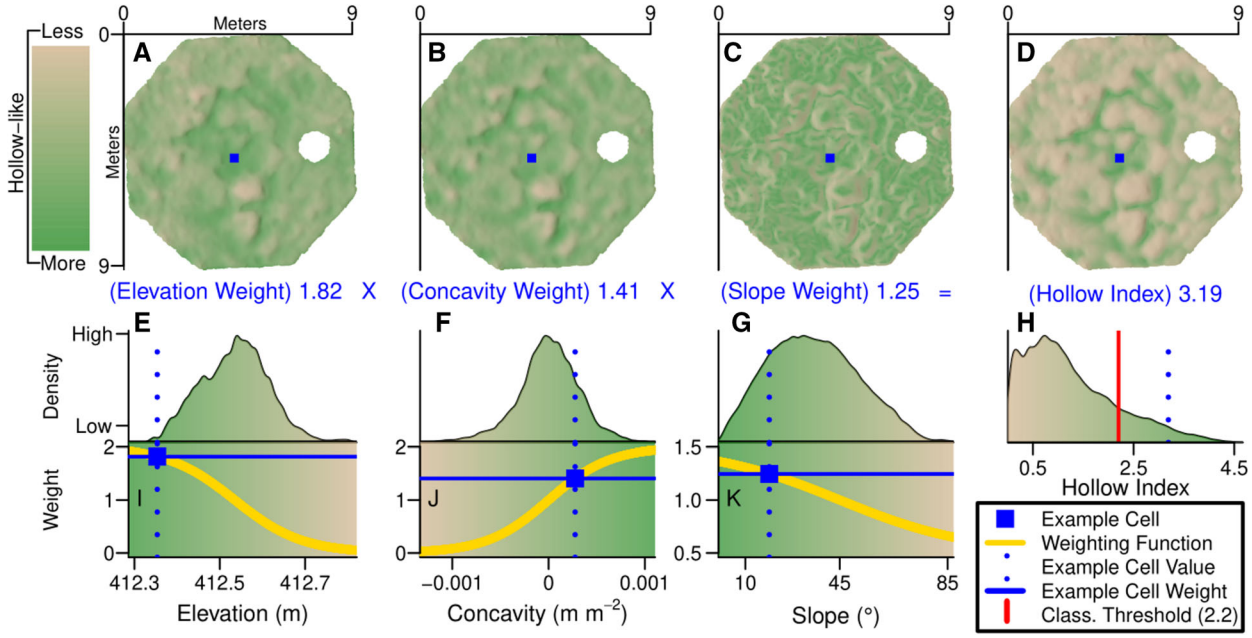


**Figure 5.** Upper panels (**A**–**D**) show maps of SPRUCE plot 7 (2017) displaying elevation, concavity, slope, and Hollow Index, respectively. The lower panel shows distributions of each variable (**E**–**H**) with the same X-axes as graphs of sigmoid weighting functions of each variable below (**I**, **J**, **K**), which are displayed on a background corresponding with map color bars. An example grid cell is displayed on maps and on sigmoid weighting function plots, showing how variable values (elevation, concavity, slope) are used in weighting functions, and how the resulting weights are multiplied to calculate the Hollow Index.

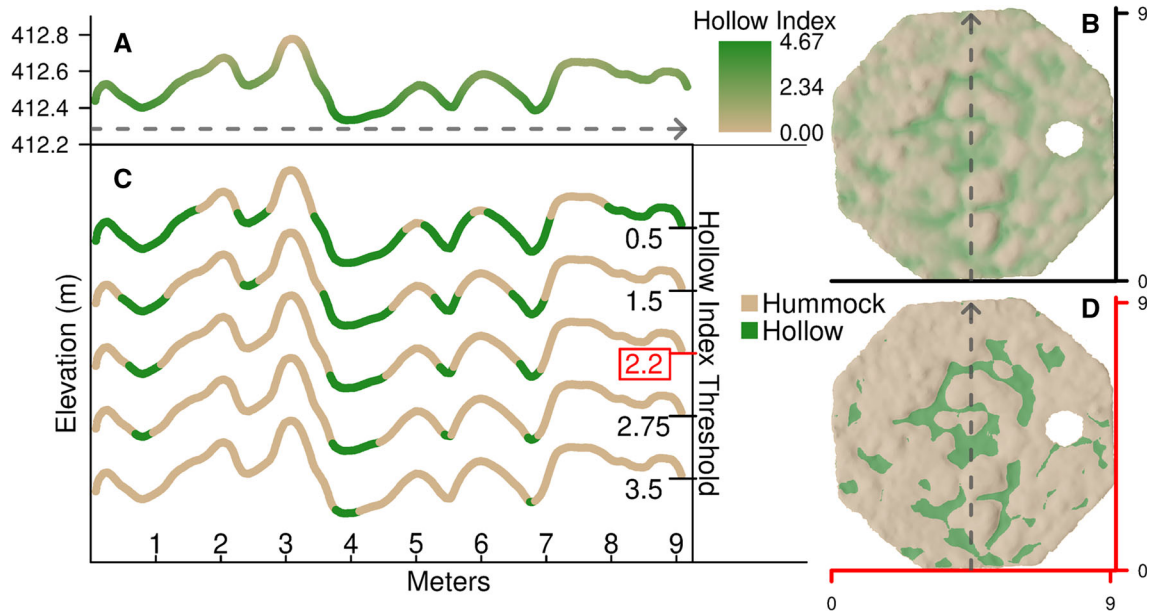


**Figure 6.** A profile of a transect (**A**) and a map (**B**) from SPRUCE plot 7 (2017) colored by the Hollow Index. The same transect classified into microforms using various Hollow Index thresholds (**C**), with a red box around the 2.2 threshold used for Scaling_Classification in this study, and the resulting microform classification map (**D**). Arrows show the location and orientation of the transect (**A**, **C**) on maps (**B**, **D**). Note that horizontal and vertical scales are not 1:1 in both A and C (that is, the lengths that represent 1 m along the *x* and *y*-axes are not equal in both panes).

the study in each plot. A Kruskal–Wallis test was used to determine if there were differences in inter-annual variability between methods. Non-parametric tests were used, because distributions were non-normal or heteroscedastic. Intra-annual (inter-plot) variability was defined as the variation in hollow percent cover of all plots within a given year, for each classification method, and was evaluated for each year of the study. Differences in intra-annual variability between methods were tested using Bartlett's tests. All statistical tests were conducted using Program R (R Core Team 2017) at $\alpha = 0.05$.

## Results

### Surface Reconstruction

The use of four scanning locations per plot reduced the effect of laser occlusion by vegetation and yielded point densities sufficient (mean > 10 points $cm^{-1}$) for high quality surface reconstructions. The Poisson surface reconstruction (Kazhdan and others 2006) performed well on the bog surface and enabled accurate reconstructions and subsequent microform classifications, even when significant noise was present. The mean absolute error of reconstructed surfaces from 357 validation points was 0.057 m (for further details on DEM accuracy see the Supplemental Material).

### Elevation Variation and Surface Roughness

Microtopography in all SPRUCE plots occurred on the scale of about 0.5–0.6 m, with the lowest elevation from all plots being − 0.48 m and the highest being +0.31 m, relative to the plot means (Figure 2). Standard deviations in DEMs elevations (that is, RR) in SPRUCE plots ranged from 0.06 to 0.08 m, with a mean = 0.07 m. Elevation distributions were typically skewed left and had positive kurtosis, with the majority of SPRUCE plots having the best fit Pearson's distribution be of type IV, although type V and VI were also best fits for individual plots. Elevation distribution from all plots combined was best fit by a Pearson's distribution IV. Pearson's distribution type and associated parameters can be found in Table 1. The range parameter for plot semivariograms ranged from 0.92 to 1.89 m (mean = 1.30 m; $\sigma = 0.30$ m) and sills ranged from 0.003 to 0.006 m (mean = 0.004 m; $\sigma = 0.001$ m). DEM roughness length ($z_0$) ranged from 0.004 to 0.005 m (mean = 0.004 m; $\sigma = 0.0005$ m). Semivariogram parameters and $z_0$ estimates can be found in Table 2.

### Microform Classifications

The three classification methods in this study had significantly different hollow coverages for all years combined ($\chi^2 = 47.55$, $df = 2$, $p < 0.001$). The 3 year mean areal coverage of hollows from Functional_Classification was intermediate (15.8%), but hollow coverages were markedly more variable than the two other methods (Figure 7). ELM_Classification produced the highest 3 year mean hollow coverage (33.8%). Hollow coverages from Scaling_Classification were the lowest and least variable (Figure 7) of the three methods, with a 3 year mean of 14.4%. Hollow coverages between methods were significantly different in all years and cases ($p < 0.05$), other than between Scaling_Classification and Functional_Classification in 2017 ($W = 68$, $df = 1$, $p = 0.84$), Functional_Classification and ELM_Classification in 2018 ($W = 41$, $df = 1$, $p = 0.08$), and Functional_Classification and Scaling_Classification in 2018 ($W = 96$, $df = 1$, $p = 0.18$).

In general, the variability (inter and intra-annually) in hollow coverage between methods followed the pattern Functional_Classification ≫ ELM_Classification > Scaling_Classification (Table 3). Intra-annual variability was significantly different ($p < 0.05$) in all cases and years except ELM_Classification and Functional_Classification in 2016 ($\chi^2 = 0.57$, $df = 1$, $p = 0.45$). There was a significant difference in plot-specific inter-annual variability of hollow percent cover (Figure 8) between classification methods ($\chi^2 = 17.21$, $df = 2$, $p < 0.001$). Non-plot-specific hollow coverage between years was only significantly different for the Functional_Classification ($\chi^2 = 10.35$, $df = 2$, $p = 0.006$), further demonstrating its higher inter-annual variability.

The higher variability in the Functional_Classification was driven primarily by differences in MWSWT between plots and years (Figure 4A, E, I), rather than structural changes in the bog surface (Figure 4B, F, J), as was the case for ELM_Classification and Scaling_Classification. This is demonstrated by the lower variability in the plot elevation distributions fifth percentiles (used in the ELM_Classification) between years (Figure 4B, F, J) compared to the relatively higher variability in MWSWT (Figure 4A, E, I). The Scaling_Classification and ELM_Classification both used only topographic data; however, Scaling_Classification was less variable than the ELM_Classification, because it incorporated multiple topographic metrics that are weighted based on plot distributions and is therefore less affected by noise from surface

**Table 1.** Parameters for Pearson's Distributions Fit to SPRUCE Plot Elevation Frequency Distributions.

| Plot | Type | Location | Scale | Par3 | Par4 |
|---|---|---|---|---|---|
| 4 | 4 | 0.24 | 0.21 | 9.64 | 19.80 |
| 6 | 6 | 0.40 | − 2.44 | 32.20 | 198.28 |
| 7 | 5 | − 0.94 | 148.56 | 159.44 | NA |
| 8 | 4 | 0.11 | 0.25 | 9.02 | 6.93 |
| 10 | 4 | 0.11 | 0.23 | 7.66 | 6.64 |
| 11 | 4 | 0.09 | 0.21 | 7.29 | 5.26 |
| 13 | 4 | 0.12 | 0.31 | 12.12 | 9.01 |
| 16 | 4 | 0.22 | 0.33 | 18.47 | 23.86 |
| 17 | 4 | 0.12 | 0.31 | 10.72 | 7.44 |
| 19 | 4 | 0.06 | 0.30 | 14.39 | 5.12 |
| 20 | 4 | 0.03 | 0.36 | 16.81 | 2.76 |
| 21 | 4 | 1.38 | 4.07 | 2602.59 | 1758.63 |
| Combined | 4 | 0.07 | 0.24 | 7.90 | 3.95 |

*When type = 4, Par3 = m and Par4 = nu; when type = 5, Par3 = Shape (no fourth parameter), when type = 6, Par3 = a and Par4 = b.*

**Table 2.** Summaries of Roughness Metrics From SPRUCE Plots

| Plot | RR (m) | SV_Sill (m) | SV_Range (m) | $z_0$ (m) | Min_Elev (m) | Max_Elev (m) |
|---|---|---|---|---|---|---|
| 4 | 0.078 | 1.34 | 0.0057 | 0.0042 | − 0.48 | 0.23 |
| 6 | 0.076 | 1.22 | 0.0056 | 0.0045 | − 0.42 | 0.22 |
| 7 | 0.075 | 0.97 | 0.0059 | 0.0049 | − 0.24 | 0.30 |
| 8 | 0.069 | 1.44 | 0.0038 | 0.0035 | − 0.37 | 0.23 |
| 10 | 0.072 | 1.36 | 0.0046 | 0.0038 | − 0.40 | 0.23 |
| 11 | 0.066 | 1.25 | 0.0040 | 0.0036 | − 0.40 | 0.24 |
| 13 | 0.072 | 1.78 | 0.0039 | 0.0043 | − 0.35 | 0.24 |
| 16 | 0.068 | 1.52 | 0.0039 | 0.0033 | − 0.39 | 0.20 |
| 17 | 0.076 | 1.59 | 0.0047 | 0.0038 | − 0.41 | 0.23 |
| 19 | 0.061 | 0.95 | 0.0037 | 0.0033 | − 0.29 | 0.20 |
| 20 | 0.066 | 1.04 | 0.0042 | 0.0037 | − 0.32 | 0.31 |
| 21 | 0.060 | 1.13 | 0.0028 | 0.0034 | − 0.34 | 0.21 |
| Combined | 0.070 | 1.30 | 0.0044 | 0.0039 | − 0.48 | 0.31 |

*RR random roughness, SV_Sill semivariogram sill, SV_Range semivariogram range, $z_0$ aerodynamic roughness length, Min_Elev minimum plot elevation relative to the mean, Max_Elev maximum plot elevation relative to the mean*

reconstructions and plot minimum elevations. This may make Scaling_Classification a preferable choice for multi-year studies which desire inter-annual consistency in microform classifications. In this study, the small changes in areal coverage of hollows between years using Scaling_Classification indicates small structural changes to the surface of the bog.

## Discussion

To our knowledge, the only published studies that quantitatively classified peatland microforms with a DEM are Lovitt and others (2018) and Stovall and others (2019). Lovitt and others (2018) used a moving window average as an elevation threshold to classify microforms (hummocks and hollows). However, our data demonstrate that elevation distributions are unimodal and not highly skewed (Figure 2). This indicates that the mean and median are similar, and therefore it is implicit that the proportion of hummocks and hollows will approximate 1:1 when using the local mean as a classification threshold. This is supported by the results in Lovitt and others (2018) who report 51.8% percent cover for hollows (48.2% hummock) in undisturbed locations. Two of our classification methods (Functional_Classification and ELM_Classification) used elevation thresholds, similar to Lovitt and others (2018). However, the elevation thresholds in this study were independent of plot elevation distributions and/or used a tolerance, which made classifications less prone to a bias toward a predetermined ratio of hummock:hollow.

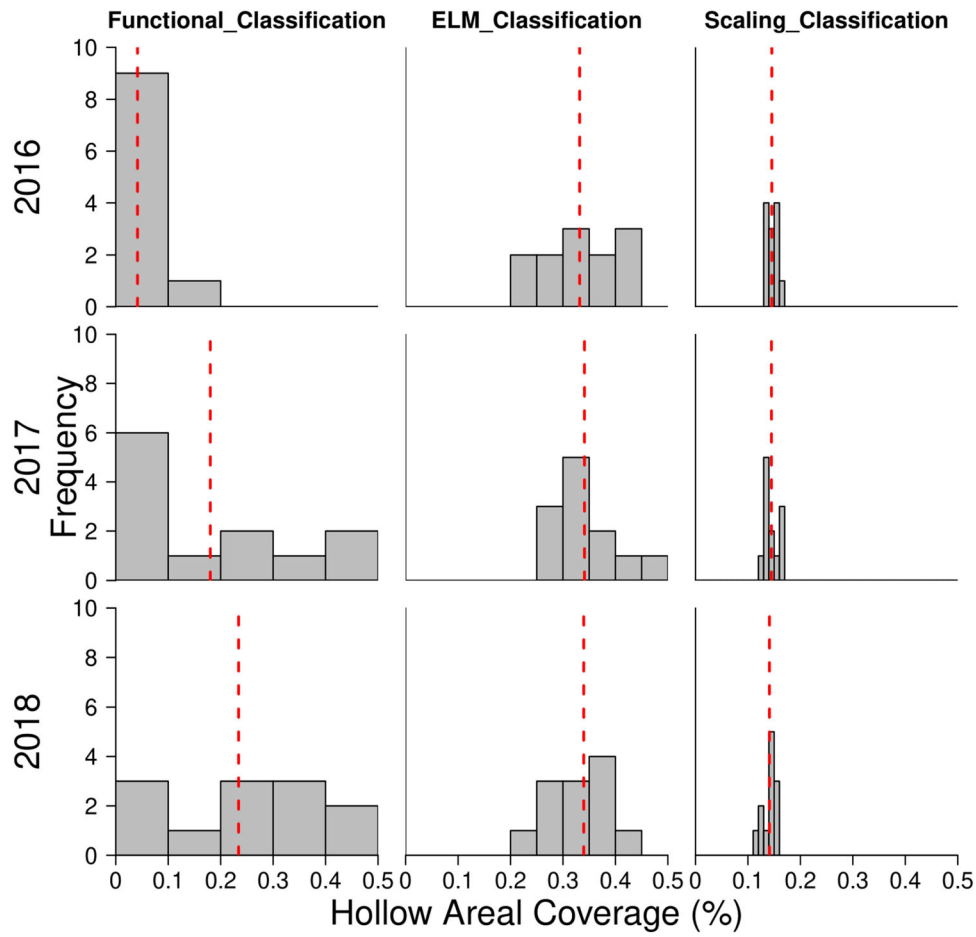


**Figure 7.** Histograms displaying the areal coverage of hollows from each classification, in all plots, in all years. Vertical red lines display means.

**Table 3.** Summary Statistics for Areal Coverage of Hollows in SPRUCE Plots by Year, and the Duration of the Study, for the All Three Classification Methods.

| Year | Statistic | Classification method (%) | | |
|---|---|---|---|---|
| | | Functional | ELM | Scaling |
| 2016 | Mean | 4.1 | 33.2 | 14.6 |
| | Range | 0.1–18.4 | 23.72–42.3 | 13.1–16.1 |
| | Standard deviation | 5.2 | 6.7 | 1.1 |
| 2017 | Mean | 18.0 | 34.1 | 14.5 |
| | Range | 0.7–43.0 | 25.42–45 | 12.5–16.5 |
| | Standard deviation | 15.9 | 5.9 | 1.3 |
| 2018 | Mean | 23.4 | 34.0 | 14.1 |
| | Range | 0.0–43.6 | 23.3–43.7 | 11.3–15.5 |
| | Standard deviation | 14.7 | 5.7 | 1.3 |
| Years combined | Mean | 15.8 | 33.7 | 14.4 |
| | Range | 0.0–43.6 | 23.3–45.0 | 11.3–16.5 |
| | Standard deviation | 15.1 | 6.0 | 1.2 |

The unimodal nature of elevation distributions in this study does not support the notion of microforms based on topography alone (at scales larger than a few meters). These results differ from those in Moore and others (2019), which reports plots exhibiting both multi-modal and unimodal eleva-

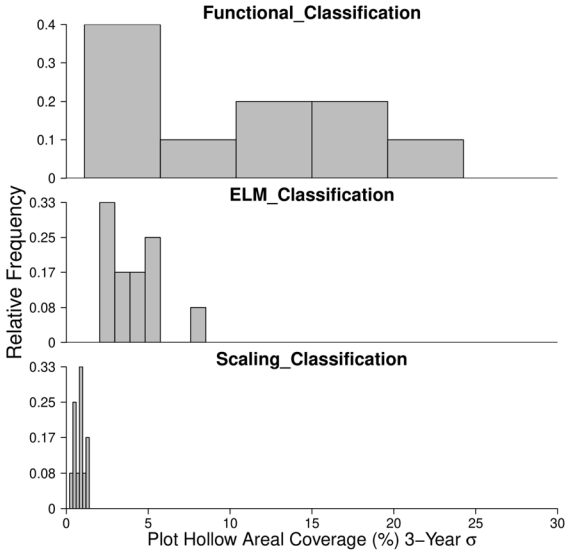


**Figure 8.** Histograms of plot-specific inter-annual variability for classification methods in all plots, calculated as the standard deviation ($\sigma$) of areal coverage of hollows for a given plot during the 3 years of the study.

tion distributions. However, the plot size in Moore and others (2019) was much smaller (3.8–10.6 $m^2$) than plots in this study (65.25–66.58 $m^2$), and some plots were specifically selected to have a distinct hummock and a distinct hollow. The discrepancy in modalities between our study and Moore and others (2019) suggest that elevation distributions may be multi-modal at small scales that approximate the size of a combination of hummock and hollow, but that the elevation distribution at scales much larger than microforms is unimodal and resembles a normal distribution. This is likely a result of microtopography having variable morphology (for example, hummock–hollow height difference and microform length/width) at the peatland level; in which elevation distributions are multi-modal at smaller scales, but when aggregated at larger scales approximate a normal distribution. This scale dependency of distribution modality is an important distinction to make for modeling applications and highlights the need to characterize microtopography at multiple scales. Future studies that sample microtopography at multiple scales in different peatland types would help elucidate inter-peatland variation and the scale dependencies of elevation distributions.

Although our data do not support the conceptualization of microforms based on form alone (that is, topography), nonlinear responses of biogeochemical processes to water table depth (for example, Rydin 1985; Moore and Knowles 1989; Schipperges and Rydin 1998; Christensen and others 2003) paired with variability in water table depth incurred by microtopography, may result in microforms that are differentiable by ecological function. Our Functional_Classification differentiated microforms by ecological function through the incorporation of water table in a manner that is representative of two nonlinear responses to water table depth. However, it should be noted that this classification likely is not representative of all relationships between biogeochemical processes and water table depth (see difference between $CH_4$ and $CO_2$ flux response to water table in Moore and Knowles 1989), but could be modified to address specific processes.

On annual timescales, classification results based purely on microform structure diverged from the Functional_Classification. This is demonstrated in Figure 4, where a relatively low warm-season water table (2016; Figure 4A) resulted in low areal coverage of hollows from the Functional_Classification (Figure 4C), and a relatively high warm-season water table (2017; Figure 4E) resulted in much higher areal coverage of hollows (Figure 4G). During this year, elevation distributions and results from the ELM_Classification were largely unchanged. This constitutes a 3 × increase in the areal coverage of hollows from the Functional_Classification in the same year that coverage from the ELM_Classification, based purely on structure, increased by only 1/10th. Large changes to areal coverage from Functional_Classification in the 3 years of this study and in the absence of major structural changes can be used to explain inter-annual variability in peatland C fluxes driven by differences in water table depth. For instance, differences in Functional_Classification areal coverage between years could be used to contextualize higher temperature response Q10 values for large-collar $CH_4$ flux measurements in 2017 and 2018 compared to 2016 from Hanson and others (2017a).

Although we focused on demonstrating how areal coverage of hollows varied between classifications, other parameters (for example, hummock height, hummock–hollow spacing, locations of hollows, and so on) also varied. This highlights the importance of parameterizing microtopography in models from data generated by classification schemes that are in accordance with the conceptualization of microforms in the model. The ELM_Classification method in this study provides a classification scheme that facilitates data-driven

parameterization of the three microtopographic parameters used in ELM_SPRUCE and models using similar representations, like the peatland carbon simulator (PCARS; Frolking and others 2002). For models which do not use a microform-based approach (for example, DigiBog in Baird and others 2011), the elevation distributions and DEMs provided in this study can be utilized to optimize elevation frequencies used to represent microtopography. Further, DEMs and measures of surface roughness reported here can be used to improve model representation of the microtopographic influence on the hydrologic cycle (for example, Jan and others 2018) and wind profiles.

This study provides data that facilitates spatial extrapolations for both measurements taken using the hummock–hollow dichotomy and along an elevation (or water table) gradient. Elevation distributions reported here combined with relationships relating biogeochemical processes to elevation or water table depth can be combined to make estimates of fluxes that will be more accurate than those made using the much more generalized microform dichotomy. However, such relationships are not always available or feasible to build. Therefore, studies using the hummock–hollow dichotomy can use our Scaling_Classification to calculate, and threshold, the continuous Hollow Index to classify microforms consistent with their placement of instrumentation in the field. Modifying the parameters and classification threshold of the Hollow Index would enable investigators to account for application-specific sampling locations, or the inherent subjectivity of investigators placing field instrumentation prior to classification. Such actions would facilitate proper scaling of measurements, by using areal coverages representative of their sampling locations.

Ideally, TLS sampling and microform mapping which would occur before field measurements are taken to ensure that appropriate locations/microforms are sampled sufficiently. SfM using handheld cameras or UAS has been proven effective for producing point clouds and DEMs of peatland microtopography (Mercer and Westbrook 2016; Lovitt and other 2018; Moore and others 2019) and could be used as a lower-cost alternative to TLS. Although SfM is not without its own challenges, UAS SfM would likely be best suited for peatlands that are treeless or have relatively low tree cover.

The differences in hollow areal coverage and the variability between classification methods clearly demonstrates how an intended purpose or application drives the conceptualization of microforms, the resulting classification, and ultimately the areal coverage (and other metrics) of microforms. Considering the marked differences in hollow areal coverage and variability between microform classifications in this study, it is evident how conclusions drawn from research utilizing microform classifications could vary widely. Using an appropriate classification is essential for producing accurate results and conclusions.

We recognize that a single method for classifying microforms is likely not sufficient to accommodate all applications. Therefore, this study provides three quantitative and explicit microform classification schemes intended to be used for different applications. The applications discussed in this study primarily focus on the microtopography–water table depth relationship and associated processes affected by the resulting soil moisture gradient. These processes occur across environmental gradients (for example, moisture, temperature, and so on) rather than in conceptual bins (hummocks and hollows), and when possible, should be represented as such. This study provides several measures of microtopography corresponding to elevation frequency distributions and spatial variability to be utilized by studies that treat microtopography as a gradient. However, quantifying these processes across gradients is not always possible, and thus requires investigators to bin or stratify their sampling. In such cases, clearly defined microforms are a necessity for inter-study comparisons and proper scaling of stratified measurements. Therefore, it is imperative to clearly define what, exactly, defines each bin.

## ACKNOWLEDGEMENTS

This material is based upon work supported by the U.S. Department of Energy, Office of Science, Office of Biological and Environmental Research. Jake Graham was supported under a contract between Oak Ridge National Laboratory and Boise State University (#4000145196) with funding for the SPRUCE project from the U.S. Department of Energy (DOE), Office of Science, Office of Biological and Environmental Research. Oak Ridge National Laboratory is managed by UT-Battelle, LLC, for DOE under contract DE-AC05-00OR22725. Additional funding was provided by the Department of Geosciences, Boise State University.

## AUTHOR CONTRIBUTIONS

JG designed the study, performed research, analyzed data, and wrote the paper. NG designed the study and wrote the paper. LS performed research and analyzed data. PH conceived of the study.

## REFERENCES

Allmaras RR, Burwell RE, Larson WE, Holt FE. 1966. Total porosity and random roughness of the interrow zone as influenced by tillage. Conservation Research Report 7. Washington, DC, USDA.

Almendinger JC, Almendinger JE, Glaser PH. 1986. Topographic fluctuations across a spring fen and raised bog in the Lost River peatland, Northern Minnesota. Journal of Ecology 74:393–401.

Andrus R, Wagner DJ, Titus JE. 1983. Vertical distribution of *Sphagnum* mosses along hummock–hollow gradients. Canadian Journal of Botany 61:3128–39.

Arsenault J, Talbot J, Moore TR, Beauvais MP, Franssen J, Roulet NT. 2019. The spatial heterogeneity of vegetation, hydrology and water chemistry in a peatland with open-water pool. Ecosystems. https://doi.org/10.1007/s10021-019-00342-4.

Baird AJ, Morris PJ, Belyea LR. 2011. The DigiBog peatland development model 1: rationale, conceptual model, and hydrological basis. Ecohydrology 5:242–55.

Benscoter BW, Wieder KR, Vitt DH. 2005. Linking microtopography with post-fire succession in bogs. Journal of Vegetation Science 16:453–60.

Brubaker KM, Myers WL, Drohan PJ, Miller DA, Boyer EW. 2013. The use of LiDAR terrain data in characterizing surface roughness and microtopography. Applied and Environmental Soil Science: Article ID 891534.

Bubier JL, Bhatia D, Moore TR, Roulet NT, Lafleur PM. 2003. Spatial and temporal spatial variability in growing-season net ecosystem carbon dioxide exchange at a large peatland in Ontario, Canada. Ecosystems 6:353–67.

Bubier J, Cotello A, Moore TR, Roulet NT, Savage K. 1993. Microtopography and methane flux in boreal peatlands, northern Ontario Canada. Canadian Journal of Botany 71:1056–63.

Campbell DR, Lavoie C, Rochefort L. 2002. Wind erosion and surface stability in abandoned milled peatlands. Canadian Journal of Soil Science 82:85–95.

Cao M, Woodward FI. 1998. Net primary and ecosystem production and carbon stocks of terrestrial ecosystems and their responses to climate change. Global Change Biology 4:185–98.

Chapin FS, Van Cleve K, Chapin MC. 1979. Soil temperature and nutrient cycling in the tussock growth form of *Eriophorum vaginatum*. Journal of Ecology 76:169–89.

Chaudhary N, Miller PA, Smith B. 2018. Biotic and abiotic drivers of peatland growth and microtopography: a model demonstration. Ecosystems 21:1196–214.

Choudhury BJ, Schmugge TJ, Chang A, Newton RW. 1979. Effect of surface roughness on the microwave emission from soils. Journal of Geophysical Research 84:5699–706.

Christensen TR, Ekberg A, Strom L, Mastepanov M, Panikov N, Oquist M, Svensson BH, Nykanen H, Martikainen PJ, Oskarsson H. 2003. Factors controlling large scale variations in methane emissions from wetlands. Geophysical Research Letters 30:1414–17.

CloudCompare (version 2.8) [GPL software]. (2017). Retrieved from http://www.cloudcompare.org/.

Currence HD, Lovely WG. 1970. The analysis of soil surface roughness. Transactions of American Society of Agricultural Engineers 13:710–14.

Damman AWH. 1978. Distribution and movement of elements in ombrotrophic peat bogs. Oikos 30:480–95.

Darboux F, Davy P, Gascuel-Odoux C, Huang C. 2002. Evolution of soil surface roughness and flowpath connectivity in overland flow experiments. Catena 46:125–39.

Darboux F, Huang C. 2003. An instantaneous-profile laser scanner to measure soil surface microtopography. Soil Science Society of America Journal 67:92–9.

Ehrenfeld JG. 1995. Microtopography and vegetation in Atlantic white cedar swamps: the effects of natural disturbances. Canadian Journal of Botany 73:474–84.

Flanagan DC, Huang C, Norton LD, Parker SC. 1995. Laser scanner for erosion plot measurements. Transactions of the American Society of Agricultural and Biological Engineers 38:703–10.

Freeman C, Lock MA, Reynolds B. 1993. Fluxes of $CO_2$, $CH_4$, and $N_2O$ form a Welsh peatland following simulation of water table draw-down: potential feedback to climatic change. Biogeochemistry 19:51–60.

Frolking S, Roulet NT, Moore TR, Lafleur PM, Bubier JL, Crill PM. 2002. Modeling seasonal to annual carbon balance of Mer Bleue Bog, Ontario, Canada. Global Biogeochemical Cycles 15:1030.

Fung I, John J, Lerner J, Matthews E, Prather M, Steele LP, Fraser PJ. 1991. Three-dimensional model synthesis of the global methane cycle. Journal of Geophysical Research 96:13033–65.

Gorham E. 1990. Biotic impoverishment in northern peatlands. In: Woodwell GM, Ed. The earth in transition: patterns and processes of biotic impoverishment. New York: Cambridge University Press. p 65–98.

Gorham E. 1991. Northern Peatlands: role in the carbon cycle and probable responses to climatic warming. Ecological Applications 1:182–95.

Graham JD, Glenn NF, Spaete LP. 2019a. SPRUCE terrestrial laser scanning of experimental plots beginning in 2015. Oak Ridge National Laboratory, TES SFA, U.S. Department of Energy, Oak Ridge, Tennessee, U.S.A. https://doi.org/10.25581/spruce.067/1515552.

Graham JD, Glenn NF, Spaete LP. 2019b. SPRUCE microtopography of experimental plots derived from terrestrial laser scans beginning in 2016. Oak Ridge National Laboratory, TES SFA, U.S. Department of Energy, Oak Ridge, Tennessee, U.S.A. https://doi.org/10.25581/spruce.068/1515553.

Griffiths NA, Sebestyen SD. 2016. Dynamic vertical profiles of peat porewater chemistry in a Northern peatland. Wetlands 36:1119–30.

Hanson PJ, Phillips JR, Riggs JS, Nettles WR. 2017a. SPRUCE Large-Collar in situ CO2 and CH4 flux data for the SPRUCE experimental plots. Whole-ecosystem-warming. Oak Ridge National Laboratory, TES SFA, U.S. Department of Energy, Oak Ridge, Tennessee, U.S.A. https://doi.org/10.3334/CDIAC/spruce.034.

Hanson PJ, Riggs JS, Nettles WR, Phillips JR, Krassovski MB, Hook LA, Gu L, Richardson AD, Aubrecht DM, Ricciuto DM, Warren JM, Barbier C. 2017b. Attaining whole-ecosystem warming using air and deep soil heating methods with an elevated $CO_2$ atmosphere. Biogeosciences 14:861–83. https://doi.org/10.5194/bg-14-861-2017.

Harris A, Baird AJ. 2018. Microtopographic drivers of vegetation patterning in blanket peatlands recovering from erosion. Ecosystems . https://doi.org/10.1007/s10021-018-0321-6.

Hirano T, Jauhiainen J, Inoue T, Takahashi H. 2009. Controls on the carbon balance of tropical peatlands. Ecosystems 6:873–87.

Huang C, Bradford JM. 1990. Portable laser scanner for measuring soil surface roughness. Soil Science Society of America Journal 54:1402–6.

Huang C, White I, Thwaite E, Bendeli A. 1988. A noncontact laser system for measuring soil surface topography. Soil Science Society of America Journal 52:350–5.

Jan A, Coon ET, Graham JD, Painter SL. 2018. A subgrid approach to modeling microtopography effects on overland flow. Water Resources Research 54:6153–67.

Johnson NL. 1949. Systems of frequency curves generated by methods of translation. Biometrika 36:149–76.

Johnson LC, Damman AWH. 1991. Species-controlled *Sphagnum* decay on a Swedish raised bog. Oikos 61:234–42.

Johnson LC, Damman AWH, Malmer N. 1990. Sphagnum macrostructure as an indicator of decay and compaction in peat cores from an ombrotrophic south Swedish peat-bog. Journal of Ecology 78:633–47.

Kamphorst EC, Jetten V, Guerif J, Pitkanen J, Iversen BV, Douglas JT, Paz A. 2000. Predicting depressional storage from soil surface roughness. Soil Science Society of America Journal 64:1749–58.

Kazhdan M, Bolitho M, Hoppe H. 2006. Poisson surface reconstruction. Symposium on Geometry Processing 61–70.

Kim J, Verma SB. 1992. Soil Surface $CO_2$ flux in a Minnesota peatland. Biogeochemistry 18:32–51.

Kuipers H. 1957. A reliefmeter for soil cultivation studies. Netherlands Journal of Agricultural Science 5:255–67.

Lettau H. 1969. Note on aerodynamic roughness-parameter estimation on the basis of roughness-element description. Journal of Applied Meteorology 8:828–32.

Lovitt J, Rahman MM, Saraswati S, McDermid GJ, Strack M, Xu B. 2018. UAV remote sensing can reveal the effect of low-impact seismic lines on surface morphology, hydrology, and methane ($CH_4$) release in a boreal treed bog. Biogeosciences 123:1117–29.

Lucieer A, Turner D, King DH, Robinson SA. 2014. Using an Unmanned Aerial Vehicle (UAV) to capture micro-topography of Antarctic moss beds. Int J Appl Earth Observ Geoinf 27:53–62.

Malhotra A, Roulet NT, Wilson P, Giroux-Bougard X, Harris LI. 2016. Ecohydrological feedbacks in peatlands: an empirical test of the relationship among vegetation, microtopography and water table. Ecohydrology 9:1346–57.

McFarlane KJ, Hanson PJ, Iversen CM, Phillips JR, Brice DJ. 2018. Local spatial heterogeneity of Holocene carbon accumulation throughout the peat profile of an ombrotrophic Northern Minnesota bog. Radiocarbon 60:941–62.

Mercer JJ, Westbrook CJ. 2016. Utrahigh-resolution mapping of peatland microform using ground-based structure from motion with multiview stereo. Journal of Geophysical Research: Biogeosciences 121:2901–16.

Miles ES, Steiner JF, Brun F. 2017. Highly variable aerodynamic roughness length ($z_0$) for a hummocky debris-covered glacier. Journal of Geophysical Research: Atmospheres 122:8447–66.

Moreno RG, Diaz Alvarez MC, Saa Requejo A, Tarquis AM. 2008. Multifractal analysis of soil surface roughness. Vadose Zone Journal 7:512–20.

Moore TR. 1989. Growth and net production of *Sphagnum* at five fen sites, subarctic eastern Canada. Canadian Journal of Botany 67:1203–7.

Moore TR, Dalva M. 1993. The influence of temperature and water table position on carbon dioxide and methane emissions from laboratory columns of peatland soils. Journal of Soil Science 44:651–64.

Moore TR, De Young A, Bubier JL, Humphreys ER, Lafleur PM, Roulet NT. 2011. A multi-year record of methane flux at the Mer Bleue Bog, Southern Canada. Ecosystems 14:646–57.

Moore TR, Knowles R. 1989. The influence of water table levels on methane and carbon dioxide emissions from peatland soils. Canadian Journal of Soil Science 69:33–8.

Moore PA, Lukenbach MC, Thompson DK, Kettridge N, Granath G, Waddington JM. 2019. Assessing the peatland hummock–hollow classification framework using high resolution elevation models: implications for appropriate complexity ecosystem modeling. Biogeosciences 16:3491–506.

Morris PJ, Baird AJ, Belyea LR. 2011a. The DigiBog peatland development model 2: ecohydrological simulations in 2D. Ecohydrology 4:256–68.

Morris PJ, Swindles GT, Valdes PJ, Ivanovic RF, Gregoire LJ, Smith MW, Tarasov L, Haywood AM, Bacon KL. 2018. Global peatland initiation driven by regionally asynchronous warming. PNAS 115:4851–6.

Morris PJ, Waddington JM, Benscoter Turetsky MR. 2011b. Conceptual frameworks in peatland ecohydrology: looking beyond the two-layered (acrotelm-catotelm) model. Ecohydrology 4:1–11.

Munir TM, Strack M. 2014. Methane flux influenced by experimental water table drawdown and soil warming in a dry boreal continental bog. Ecosystems 7:1271–85.

Nouwakpo SN, James MR, Weltz MA, Huang CH, Chagas I, Lima L. 2014. Evaluation of structure from motion for soil microtopography. Photogramm Rec 29:297–316.

Nouwakpo SK, Weltz MA, McGwire KC. 2016. Assessing the performance of structure-from-motion photogrammetry and terrestrial LiDAR for reconstructing soil surface microtopography of naturally vegetated plots. Earth Surf Proc Land 41:308–22.

Nungesser MK. 2003. Modelling microtopography in boreal peatlands: hummocks and hollows. Ecological Modelling 165:175–207.

Pearson K. 1895. Contributions to the mathematical theory of evolution, II: skew variation in homogeneous material. Philosophical Transactions of the Royal Society 186:343–414.

Pearson K. 1901. Mathematical contributions to the theory of evolution, X: supplement to a memoir on skew variation. Philosophical Transactions of the Royal Society 197:287–99.

Pearson K. 1916. Mathematical contributions to the theory of evolution, XIX: second supplement to a memoir on skew variation. Philosophical Transactions of the Royal Society 216:538–48.

Post RM, Emanuel WR, Zinke PJ, Stangenberger AG. 1982. Soil carbon pools and world life zones. Nature 298:156–9.

Pouliot R, Rochefort L, Karofeld E. 2011. Initiation of microtopography in revegetated cutover peatlands. Applied Vegetation Science 14:158–71.

R Core Team. 2017. R: a language and environment for statistical computing. R Foundation for Statistical Computing, Vienna, Austria. https://www.R-project.org/.

Rydin H. 1985. Effect of water level on desiccation of Sphagnum in relation to surrounding Sphagna. Oikos 45:374–9.

Scharlemann PW, Tanner EVJ, Hiederer R, Kapos V. 2014. Global soil carbon: understanding and managing the largest terrestrial carbon pool. Carbon Management 5:81–91. https://doi.org/10.4155/cmt.13.77.

Schipperges B, Rydin H. 1998. Response of photosynthesis of Sphagnum species from contrasting microhabitats to tissue water content and repeated desiccation. New Phytologist 140:677–84.

Sebestyen SD, Dorrance C, Olson DM, Verry ES, Kolka RK, Elling AE, Kyllander R. 2011. Longterm monitoring sites and trends at the Marcell Experimental Forest. In: Kolka RK, Sebestyen SD, Verry ES, Brooks KN, Eds. Peatland biogeochemistry and watershed hydrology at the Marcell experimental forest. Boca Raton (FL): CRC Press. p 15–72.

Shi X, Thornton PE, Ricciuto DM, Hanson PJ, Mao J, Sebestyen SD, Griffiths NA, Bisht G. 2015. Representing northern peatland microtopography and hydrology within the Community Land Model. Biogeosciences 12:6463–77.

Slater L, Hanson PJ, Hook LA. 2012. SPRUCE S1 Bog Peat Depth Determined by Push Probe and GPR: 2009–2010. Oak Ridge National Laboratory, TES SFA, U.S. Department of Energy, Oak Ridge, Tennessee, U.S.A. https://doi.org/10.3334/CDIAC/spruce.002.

Smith MW, Quincey DJ, Dixon T, Bingham RG, Carrivick JL, Irvine-Fynn TDL, Rippin DM. 2016. Aerodynamic roughness of glacial ice surfaces from high-resolution topographic data. Journal of Geophysical Research: Earth Surface 121:748–66.

Smith MV, Warburton J. 2018. Microtopography of bare peat: a conceptual model and objective classification from high-resolution topographic survey data. Earth Surface Processes and Landforms 43:1557–74.

Stovall AEL, Diamond JS, Slesak RA, McLaughlin DL, Shugart H. 2019. Quantifying wetland microtopography with terrestrial laser scanning. Remote Sensing of Environment 232:111271.

Sullivan PF, Arens SJT, Chimner RA, Welker JM. 2008. Temperature and microtopography interact to control carbon cycling in a high Arctic fen. Ecosystems 11:61–76.

Vermang J, Norton LD, Baetens JM, Huang C, Cornelis WM, Gabriels D. 2013. Quantification of soil surface roughness evolution under simulated rainfall. Transaction of the American Society of Agricultural and Biological Engineers 56:505–14.

Waddington JM, Roulet NT. 1996. Atmosphere-wetland carbon exchanges: scale dependency of $CO_2$ and $CH_4$ exchange on the developmental topography of a peatland. Global Biogeochemical Cycles 10:233–45.

Walker AJ, Carter KR, Gu L, Hanson PJ, Malhotra A, Norby RJ, Sebestyen SD, Wullschleger SD, Weston DJ. 2017. Biophysical drivers of seasonal variability in Sphagnum gross primary production in a northern temperate bog. Journal of Geophysical Research: Biogeosciences 122:1078–97.

Weltzin JF, Harth C, Bridham SD. 2001. Production and microtopography of bog bryophytes: response to warming and water-table manipulations. Oecologia 128(557):656.

Yu Z. 2011. Holocene carbon flux histories of the world's peatlands: global carbon-cycle implications. The Holocene 21:761–74.

Yu Z. 2012. Northern peatland carbon stocks and dynamics: a review. Biogeosciences 9:4071–85.

Yu Z, Beilman DW, Frolking S, MacDonald GM, Roulet NT, Camill P, Charman DJ. 2011. Peatlands and their role in the global carbon cycle. EOS 92:97–108.

Yu ZC, Loisel J, Brosseau DP, Beilman DW, Hunt SJ. 2010. Global peatland dynamics since the Last Glacial Maximum. Geophysical Research Letters 37:L13402.